



ELSEVIER Applied Mathematics and Computation 152 (2004) 725–742

Available at
www.ElsevierMathematics.com
POWERED BY SCIENCE @ DIRECT®

APPLIED
MATHEMATICS
AND
COMPUTATION

www.elsevier.com/locate/amc

Optimal multigrid solutions of two-dimensional convection–conduction problems

Maximilian S. Mesquita, Marcelo J.S. de Lemos *

*Departamento de Energia, IEME, Instituto Tecnológico de Aeronáutica, ITA-CTA,
12228-900 São José dos Campos, SP, Brazil*

Abstract

The present work investigates the efficiency of the multigrid numerical method when used to solve two-dimensional laminar velocity and temperature fields inside a rectangular domain. Numerical analysis is based on the finite volume discretization scheme applied to structured orthogonal regular meshes. Performance of the correction storage (CS) multigrid algorithm is compared for different inlet Reynolds number (Re_{in}) and number of grids. Up to four grids were used for both V - and W -cycles. Simultaneous and uncoupled temperature–velocity solution schemes were investigated. Advantages in using more than one grid are discussed. For simultaneous solution, results further indicate an increase in the computational effort for higher inlet Reynolds number Re_{in} . Optimal number of intermediate relaxation sweeps for within both V - and W -cycles is discussed upon.

© 2003 Elsevier Inc. All rights reserved.

Keywords: Multigrid; Numerical methods; CFD; Laminar flow; Decoupled solution

1. Introduction

Generally speaking, convergence rates of single-grid numerical solutions are greatest in the beginning of calculations, slowing sensibly as the iterative process goes on. Such effect gets more pronounced as the mesh becomes

* Corresponding author.

E-mail address: delemos@mec.ita.br (M.J.S. de Lemos).

Nomenclature

L_y	domain height
L_x	domain length
M	maximum number of grids
P	pressure
Pr	Prandtl number
R_{ij}	residue for continuity equation
R_T	residue for energy equation
Re	Reynolds number
S_ϕ	source term for variable ϕ , $\phi = U, V, T$
T	temperature
U	velocity component in x -direction
V	velocity component in y -direction
x	streamwise coordinate
y	transverse coordinate

Subscripts

i, j	nodal indices for volume centered variables
in	inlet value
k	grid level
nb	neighbor
T	temperature

Greeks

μ	fluid dynamic viscosity
ρ	fluid density
ϕ	general dependent variable, $\phi = U, V, T$
ν^{cg}	number of domain sweeps in the coarsest grid
ν^{pre}	number of domain sweeps before <i>restriction</i>
ν^{post}	number of domain sweeps after <i>prolongation</i>

refined. Large grid sizes, however, are often needed when capturing thin boundary layer properties, resolving small recirculating regions or detecting high heat transfer spots.

The reason for that *hard-to-converge* behavior is that iterative methods can efficiently smooth out only those Fourier error components of wavelengths smaller than or comparable to the grid size. In contrast, the multigrid method aims to cover a broader range of wavelengths through relaxation on more than one grid.

The number of iterations and convergence criterion in each step along consecutive grid levels visited by the algorithm determines the so-called V - and

W-cycles. Within each cycle, the intermediate solution is relaxed before (*pre*-) and after (*post-smoothing*) the transportation of values to coarser (*restriction*) or to finer (*prolongation*) grids [1,2,13].

Accordingly, multigrid methods have been used in an ever greater number of calculations presented in the literature and can be roughly classified into two major categories. In the CS formulation, algebraic equations are solved for the *corrections* of the variables whereas, in the *full approximation storage* (FAS) scheme, the *variables* themselves are handled in all grid levels. It has been pointed out in the literature that the application of the CS formulation is recommended for the solution of linear problems being the FAS formulation more suitable to non-linear cases [1,2,13]. An exception to this rule seems to be the work of Jiang et al. [5], who reported predictions for the Navier–Stokes equations successfully applying the multigrid CS formulation. In the literature, however, not too many attempts in solving non-linear problems with multigrid linear operators are found.

Acknowledging the advantages in using multiple grids, Rabi and de Lemos [8], presented numerical computations applying this technique to recirculating flows in several geometries of engineering interest. There, the *correction storage* (CS) formulation, motivated by the previous attempt of Jiang et al. [5], was applied to non-linear problems. Later, Rabi and de Lemos [9], analyzed the effect of *Peclet* number and the use of different solution cycles when solving the temperature field within flows with a given velocity distribution. In all those cases, the advantages in using more than one grid in iterative solutions were confirmed. More recently, Rabi and de Lemos [10,11] presented a study on optimal convergence characteristics in solution of conductive–convective problems with a given velocity field [10] and in isothermal flow simulations [11].

The present contribution extends the early work on optimization of convergence acceleration of multigrid solutions, considering now the energy equation. More specifically, a heated steady-state flow in a symmetric tank is analyzed with up to four grids. Also presented are solutions for a backward facing step flow. A schematic of such configurations is shown in Fig. 1. The numerical method includes finite volume discretization, the SIMPLE pressure–velocity coupling [6] and the Three-Diagonal Matrix Algorithm (TDMA). The overall algorithm performance is discussed in light of computational effort required.

2. Mathematical model and numerics

2.1. Governing equations

The continuity, Navier–Stokes and energy equations describe fluid flow and heat transfer. They express mass, momentum and energy conservation

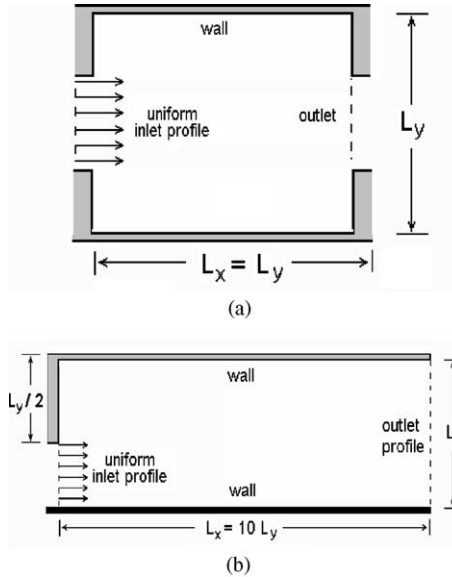


Fig. 1. Geometries and boundary conditions for (a) heated flow in a tank, (b) back step heated flow.

principles respectively and, for a steady state condition in a two-dimension Cartesian coordinate frame, they are written as:

$$\frac{\partial}{\partial x}(\rho U) + \frac{\partial}{\partial y}(\rho V) = 0, \quad (1)$$

$$\frac{\partial}{\partial x}(\rho U^2) + \frac{\partial}{\partial y}(\rho VU) = \frac{\partial}{\partial x}\left(\mu \frac{\partial U}{\partial x}\right) + \frac{\partial}{\partial y}\left(\mu \frac{\partial U}{\partial y}\right) - \frac{\partial P}{\partial x}, \quad (2)$$

$$\frac{\partial}{\partial x}(\rho UV) + \frac{\partial}{\partial y}(\rho V^2) = \frac{\partial}{\partial x}\left(\mu \frac{\partial V}{\partial x}\right) + \frac{\partial}{\partial y}\left(\mu \frac{\partial V}{\partial y}\right) - \frac{\partial P}{\partial y}, \quad (3)$$

$$\frac{\partial}{\partial x}(\rho UT) + \frac{\partial}{\partial y}(\rho VT) = \frac{\partial}{\partial x}\left(\frac{\mu}{Pr} \frac{\partial T}{\partial x}\right) + \frac{\partial}{\partial y}\left(\frac{\mu}{Pr} \frac{\partial T}{\partial y}\right), \quad (4)$$

where ρ is the fluid density, U and V are the x and y velocity components, respectively, T is the temperature, μ is the dynamic viscosity and Pr is the Prandtl number. In addition, in this work all fluid properties are held constant.

2.2. Numerical model

The solution domain is divided into a number of rectangular control volumes (CV), resulting in a structured orthogonal non-uniform mesh. Grid

In (7) $D_e = \mu_e \delta y / \Delta x_e$ and $C_e = (\rho U)_e \delta y$ are the diffusive and convective fluxes at the CV east face, respectively, and, as usual, the operator $\max[a, b]$ returns the greater of a and b .

2.3. Multigrid technique

Assembling equation (6) for each control volume of Fig. 2 in the domain of Fig. 1 defines a linear algebraic equation system of the form,

$$\mathbf{A}_k \mathbf{T}_k = \mathbf{b}_k, \tag{8}$$

where \mathbf{A}_k is the *matrix of coefficients*, \mathbf{T}_k is the *vector of unknowns* and \mathbf{b}_k is the vector accommodating source and extra terms. Subscript “ k ” refers to the grid level, with $k = 1$ corresponding to the coarsest grid and $k = M$ to the finest mesh.

As mentioned, multigrid is here implemented in a CS formulation in which one seeks coarse grid approximations for the *correction* defined as $\delta_k = \mathbf{T}_k - \mathbf{T}_k^*$ where \mathbf{T}_k^* is an *intermediate value* resulting from a small number of iterations applied to (8). For a linear problem, one shows that δ_k is the solution of [1,2,13],

$$\mathbf{A}_k \delta_k = \mathbf{r}_k, \tag{9}$$

where the *residue* is defined as

$$\mathbf{r}_k = \mathbf{b}_k - \mathbf{A}_k \mathbf{T}_k^*. \tag{10}$$

Eq. (9) can be approximated by means of a coarse-grid equation,

$$\mathbf{A}_{k-1} \delta_{k-1} = \mathbf{r}_{k-1} \tag{11}$$

with the *restriction operator* I_k^{k-1} used to obtain

$$\mathbf{r}_{k-1} = I_k^{k-1} \mathbf{r}_k. \tag{12}$$

The residue restriction is accomplished by summing up the residues corresponding to the four fine grid control volumes that compose the coarse grid cell. Thus, Eq. (12) can be rewritten with the help of Fig. 3 as,

$$r_{k-1}^{IJ} = r_k^{ij} + r_k^{ij+1} + r_k^{i+1j} + r_k^{i+1j+1}. \tag{13}$$

Diffusive and convection coefficients in matrix \mathbf{A}_k need also to be evaluated when changing grid level. Diffusive terms are recalculated since they depend upon neighbor grid node distances whereas coarse grid mass fluxes (*convective terms*) are simply added up at control volume faces. A schematic of this operation, commonly found in the literature [3,7], is shown in Fig. 3.

Once the coarse grid approximation for the correction δ_{k-1} has been calculated, the *prolongation operator* I_{k-1}^k takes it back to the fine grid as

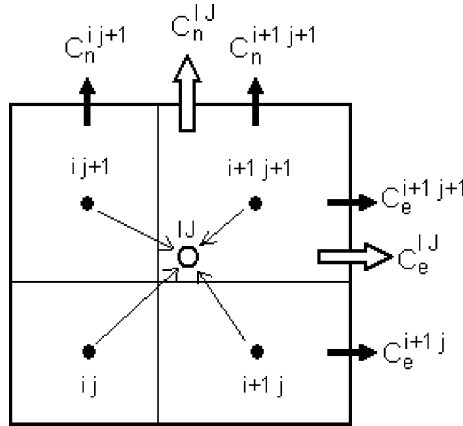


Fig. 3. Mass flux and residue restriction summation.

$$\delta_k = I_{k-1}^k \delta_{k-1} \tag{14}$$

in order to update the intermediate value

$$\mathbf{T}_k = \mathbf{T}_k^* + \delta_k. \tag{15}$$

Fig. 4 illustrates a 4-grid iteration scheme for both the *V*- and *W*-cycles where the different operations are: *s* = smoothing, *r* = restriction, *cg* = coarsest grid iteration and *p* = prolongation. Also, the number of domain sweeps before and after grid change is denoted by v^{pre} and v^{post} , respectively. In addition, at the coarsest k level ($k = 1$), the grid is swept v^{cg} times by the error smoothing operator.

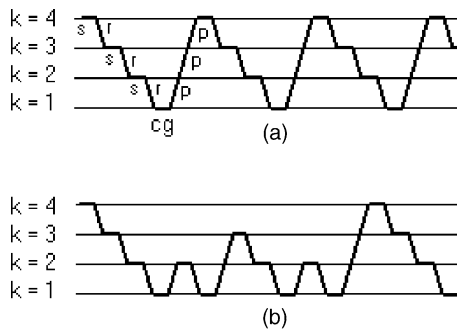


Fig. 4. Sequence of operations in a 4-grid iteration (a) *V*-cycle; (b) *W*-cycle.

3. Results and discussion

3.1. Computational details

The computer code developed was run on a IBM PC machine with a Pentium 166 MHz processor. Grid independence studies were conducted such that the solutions presented herein are essentially grid independent. For both V - and W -cycles, pre- and post-smoothing iterations were accomplished via the Gauss–Seidel algorithm while, at the coarsest-grid, the TDMA method has been applied [6]. Also, cases (a) and (b) in Fig. 1 were run with the finest grid having sizes 66×66 and 144×48 , respectively.

Results below are focused on the behavior of the energy equation subjected to multigrid numerical methods. Analysis of velocity and pressure convergence characteristics have already been reported [8,11] and for that they are here not discussed.

3.2. Numerical accuracy

This work has been mostly concerned with the performance of the multigrid method in heated recirculating flows, rather than obtaining the absolute temperature distribution. Nevertheless, care was taken when discretizing the governing equations and applying the algorithm selected. In addition to grid independence tests mentioned above, tests were conducted in order to assure the correctness of the computer code developed and the accuracy of the solution obtained. For this purpose, the heat tank geometry in Fig. 1(a) was chosen. The inlet opening on the left and the exit on the right are centered half way between the top and bottom walls, besides being of the same size. In addition, boundary conditions for temperature were also symmetric in relation to the mid plane located at height $L_y/2$. With that, calculated velocity and temperature fields, if successfully converged, had to exhibit symmetry along y .

Numerical values for U , V , P and T were symmetric up to the *fifth* decimal figure the least, and the residue of Eq. (6) was brought down to 1×10^{-16} . Although no direct comparison with experiments are included herein, residue levels essentially “touching” the double precision limit of the machine used, and perfectly symmetric values, have given the authors confidence on results here shown.

3.3. Temperature field

Fig. 5 show non-dimensional temperature distribution patterns for flow in the tank of Fig. 1(a). All walls are kept at the same temperature, higher than the incoming flow temperature. The figure indicates the effect of increasing the inlet Reynolds number, $Re_{in} = \rho U_{in} L_{in} / \mu$, where the subscript “in” refers to

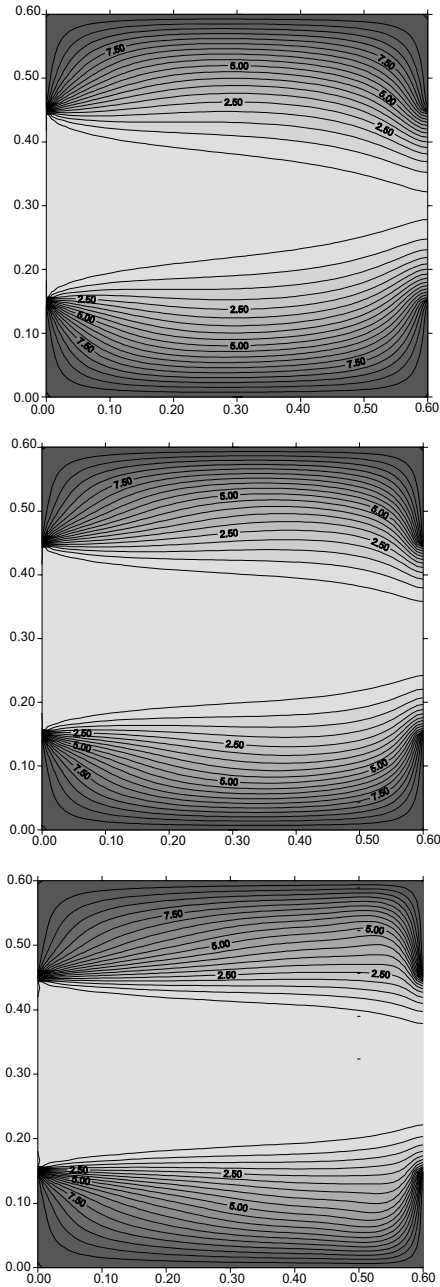


Fig. 5. Effect of Re_{in} on temperature pattern inside the heated tank of Fig. 1. From top to bottom: $Re_{in} = 75, 150, 300$.

inlet values. One can clearly see the cooling of the outlet flow as Re_{in} increases. Also interesting to note is the higher temperature gradients at the right wall, indicating a higher heat load to the solid material.

Similar results for the backward facing step are also shown in Fig. 6 where non-dimensional temperature distribution for the sudden expansion flow of Fig. 1(b) is presented. All walls are kept at the same temperature, higher than the incoming flow temperature. Here again the figure indicates the effect of increasing the inlet Reynolds number. One can also clearly see the penetration of the cooler fluid as Re_{in} increases. Deformation of the isotherms close to the step, at the upper left region, indicates the increase of the recirculation bubble after the expansion. When designing heat transfer equipment, engineers may use such information for improving product reliability and performance.

3.4. Residues

The residue is normalized and calculated according to

$$R_T = \sqrt{\sum_{ij} (R_{ij}^2)} \quad \text{with} \quad R_{ij} = A_p T_p - \left(\sum_{nb} A_{nb} T_{nb} \right), \quad (16)$$

where subscript ij identifies a given control volume on the finest grid and nb refers to its neighboring control volumes.

Fig. 7 shows residue history for the backward facing step case following the two cycles picture on Fig. 4, namely the V - and W -cycles. The solution follows a simultaneous approach in the sense that the temperature is always relaxed after the flow field, within the multigrid cycle. One can readily notice for both

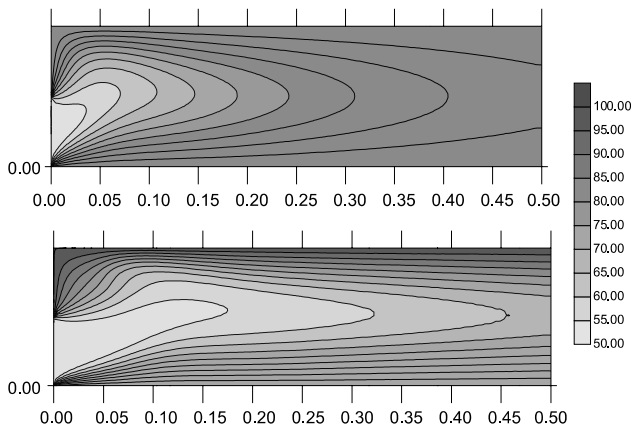


Fig. 6. Effect of Re_{in} on temperature pattern for backward facing step of Fig. 1. From top to bottom: $Re_{in} = 100, 400$.

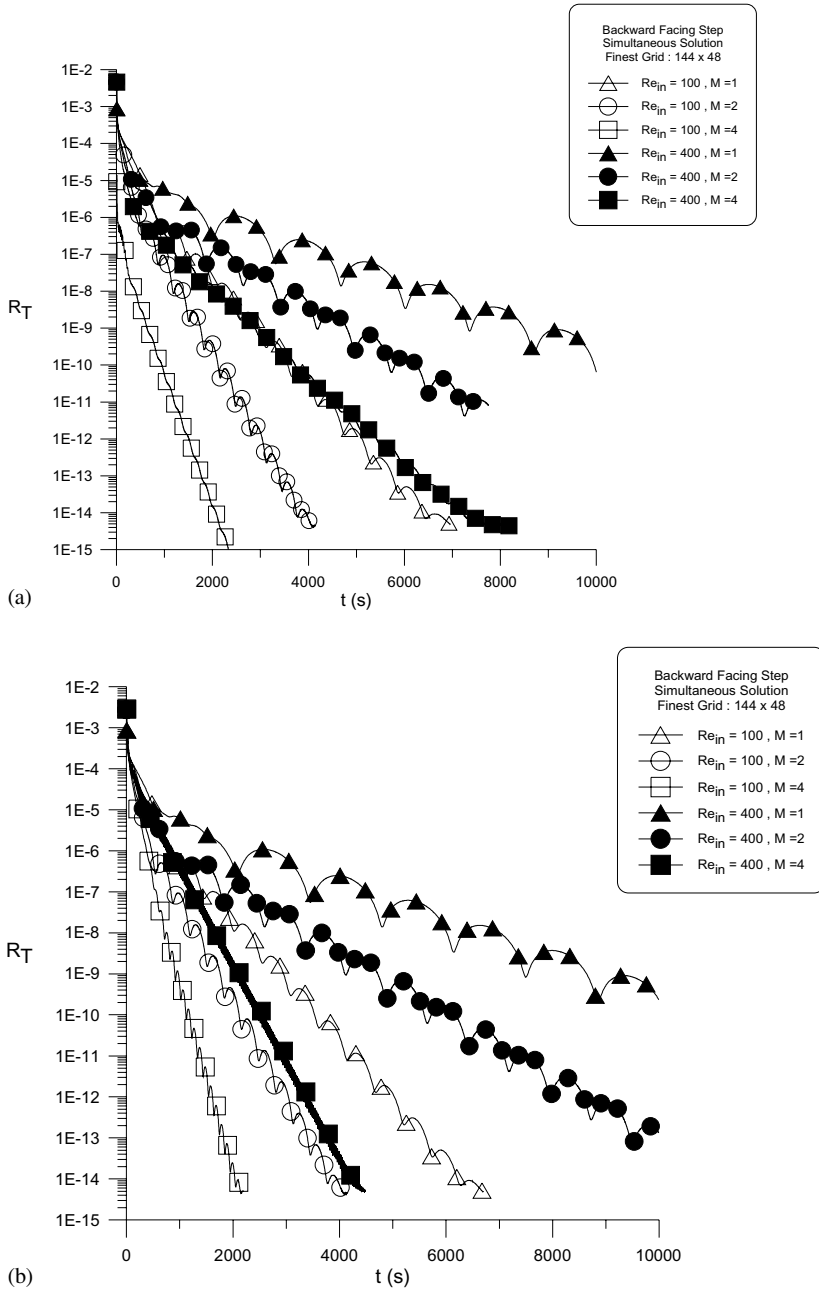


Fig. 7. Residue history for different number of grids and Re_{in} (a) V -cycle, (b) W -cycle.

cycles that for a lower Re_{in} , regardless of the number of grids used, faster solutions are obtained. In this case, relative importance of diffusion terms favors the stability of the system of equations. Increasing the number of grids for the same Reynolds number is also advantageous. This feature is what makes multigrid methods attractive, justifying their growing usage. Also interesting to note is that for the V -cycle and for $Re_{in} = 400$ (Fig. 7(a)), the computational effort related to value transfers among too many grids became relevant. Using a W -cycle (Fig. 7(b)) for this Reynolds seems to bring more savings to the iterative simultaneous solution procedure. When recalling the nature of the W -cycle in comparison with the V strategy (Fig. 4), one can see that the number of grid transfers per cycle is less in the former algorithm. In addition, the more work done in the lower frequency range of the error spectrum with the W -cycle contributes for a faster overall solution. As will be seen later, this will not be the case when the solution considers only the temperature field, given a known flow distribution. Fig. 7 also indicates the advantage in using more grids, in both cycles.

Recognizing that the situation here investigated embraces physical uncoupling between momentum and heat transfer, i.e., heat transfer depends on flow, not the other way around, an “uncoupled” algorithm has been devised. In this case, the flow field is obtained first and is recorded. Subsequently, the multigrid method is applied to the energy equation only, having the convection strength calculated with the stored flow field. Also, noting that the computational time may not be a universal parameter when comparing calculations in a variety of machines, the following residue history was monitored considering the number of iterations (full cycle in Fig. 4), rather than computational time. Fig. 8 presents residue history for the energy equation for the two situations considered, namely the simultaneous multigrid solution for velocity and temperature and the sole solution of the energy equation, given the flow field. As expected, the number of iterations needed in the latter case is lower, being nearly one order of magnitude less than in the former. Consequently, the advantage in using multiple grids is felt stronger in simultaneous solutions where overall computing time is greater.

3.5. Optimal relaxation parameters

In the work of Rabi and de Lemos [10,11], a study was carried out to investigate optimal values for the parameters ν^{pre} , ν^{post} and ν^{cg} . Since the intermediate solutions, before and after grid changes, are not fully solved but are rather relaxed ν^{pre} and ν^{post} times, a question about their optimal values for increasing overall algorithm performance arises. Or say, as restriction and prolongation operations may also introduce imprecision to values being transferred, one should expect the computational effort to be sensitive to the number of smoothing sweeps. In other words, once the intermediate numerical

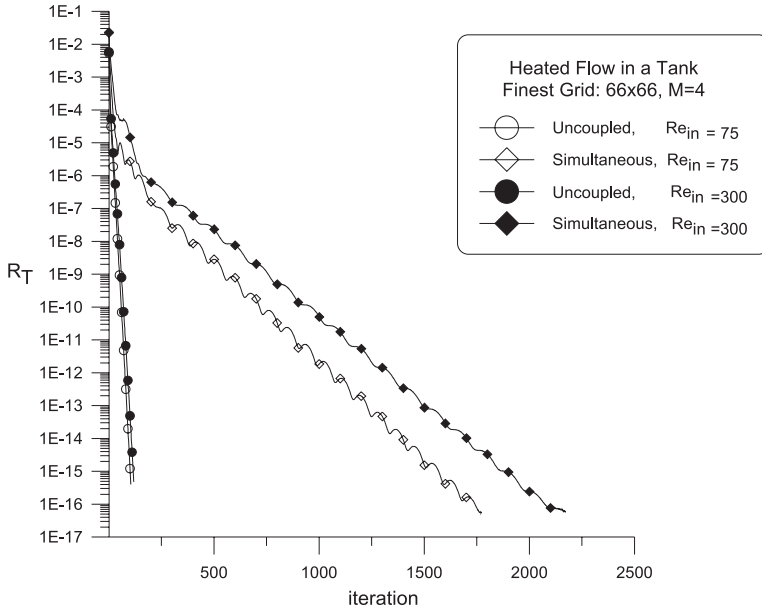


Fig. 8. Effect of field decoupling on residue history for energy equation.

solution has been relaxed a number of times removing errors introduced by the transfer operators and further reducing the residue, it is of no use to keep iterating at a certain grid level. The next figures help to analyze the existence of such optimal intermediate smoothing.

For a fixed number of sweeps at the coarse grid Fig. 9 reproduces the necessary time to convergence when the number of pre- and post-smoothing iterations was allowed to vary, keeping $\nu^{pre} = \nu^{post}$. Fig. 9(a) show results for the heated tank case with $\nu^{cg} = 7$ and 10, whereas Fig. 9(b) presents similar results for backward facing step.

In Fig. 9(a) one can see that more than one sweep for relaxing the intermediate solution, before and after grid change, brings no advantage to the algorithm performance and, consequently, further relaxation past this limit unnecessarily increases the computational effort. The advantage in using W -cycles is also apparent. In addition, for the two values of ν^{cg} used (6 and 10), no detectable savings in computational time, for both cycles, are seen.

On the other hand for the backward step case and for a fixed number of sweeps at the coarse grid ($\nu^{cg} = 15$), Fig. 9(b) clearly shows optimal values for those relaxation parameters. Additional sweeps past those values consume extra computing time. Also, too few pre- and post-relaxation passes will demand also a higher computational effort. Comparing with the previous case (a) in this figure, the use of the V -cycle shows advantages for the backward facing

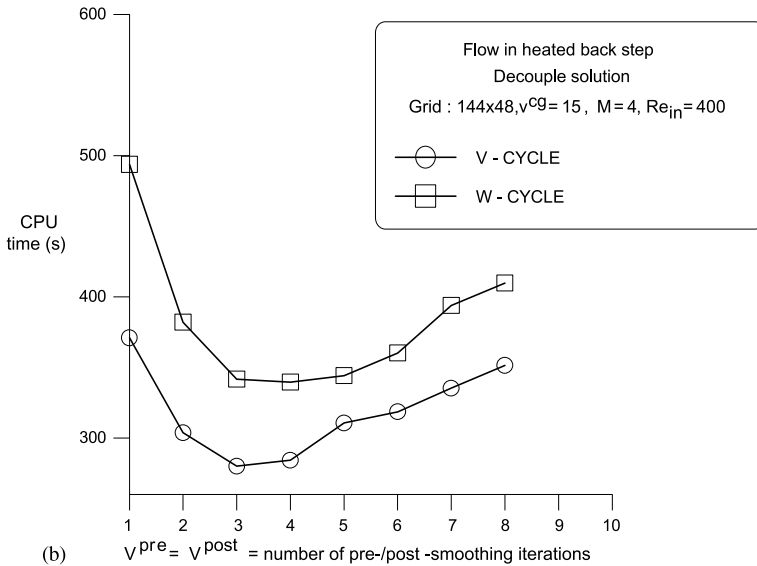
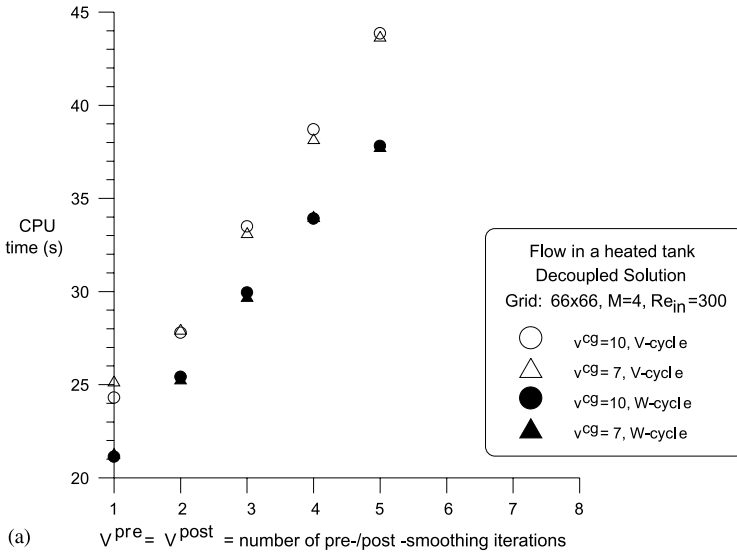


Fig. 9. Influence of the number of pre/post-smoothing iterations on the computational effort, (a) heated flow in a tank, (b) back step heated flow.

step case. This might be an indication of a dependence of the optimal cycling strategy on the flow geometry and boundary conditions. It is also important to emphasize that the case in Fig. 9(b) is different from that of Fig. 7 where a

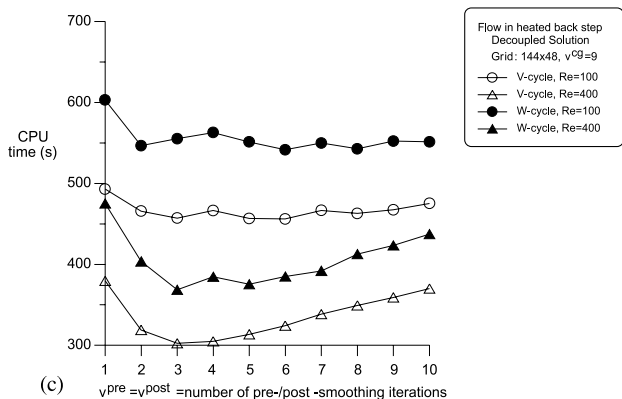
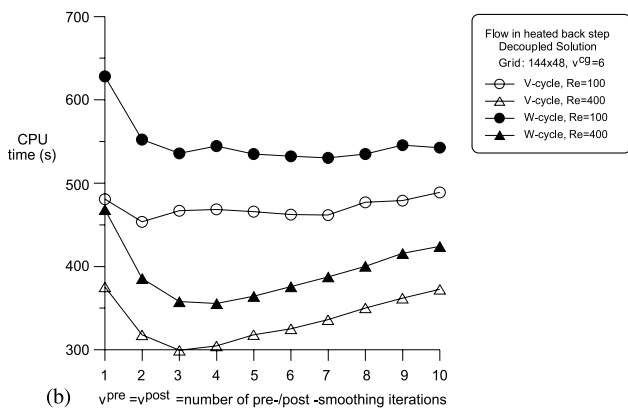
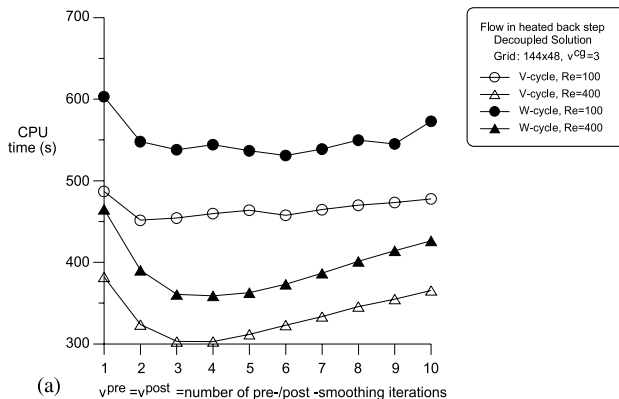


Fig. 10. Influence of the number of pre/post-smoothing iterations (a) $v^{CG} = 3$, (b) $v^{CG} = 6$, (c) $v^{CG} = 9$.

“simultaneous” solution was used. To investigate the sensitivity of the optimal value to the flow Reynolds number, Fig. 10 presents the necessary convergence times for different Re and ν^{cg} . In all decoupled solutions for the back step flow, relaxation along a V -cycle was more efficient. The dependence with Re is also similar to that of Fig. 7. Also, for the range of ν^{cg} used in this figure, no detectable

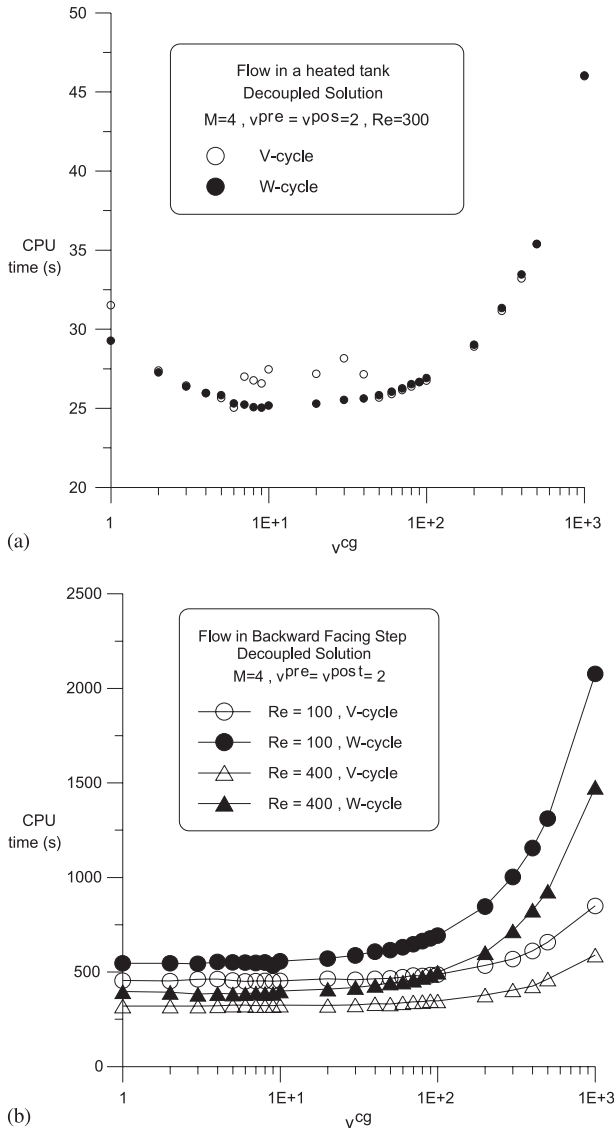


Fig. 11. Influence of the number of coarsest-grid iterations, ν^{cg} , on the computational effort.

differences on computational effort were found. All of these results raises the question of how the value of ν^{cg} affects convergence performance as well.

In Fig. 11 the number of pre- and post-smoothing iterations was fixed at $\nu^{pre} = \nu^{post} = 2$ whereas the number of coarsest-grid sweeps ν^{cg} was free to vary. For flow in the heated tank (Fig. 11(a)), an optimum situation can be clearly identified for both cycles and further relaxation past this limit brings no time savings. Here again the superiority of the W -cycle for the tank case is apparent, but only for a short range of ν^{cg} . In Fig. 11(b) no minimum value for the number of sweeps at the coarsest grid was detected. Only one pass through the domain is enough for obtaining best results. Here again the two flow considered behave differently as far as optimal values for ν^{cg} is of concern.

Ultimately, both Figs. 9–11 suggest a delicate balance between all parameters involved when minimum CPU consumption is sought. Most often, optimal parameters can not be easily determined a priori and adaptive strategies have been proposed in the literature. Generally, the ratio of residues after two successive sweeps is monitored and used as a criterion for switching grids. Hortmann et al. [3] points out that this practice is preferred for single equation systems but, when solving the full equation set as done here, such practice is not easy to implement. In this case, most works in the literature specify a fixed number of sweeps, as in the cases here reported [4,12].

4. Concluding remarks

The multigrid method has been implemented in a CS manner to numerically solve a two-dimensional steady-state conduction–convection problem. Structured, orthogonal and regular meshes were used and discretized equations were obtained through a finite volume formulation. The overall algorithm performance was compared for different inlet Reynolds numbers, for distinct cycles, for different number of intermediate solution sweeps and coarsest-grid iterations.

Results proved the superiority of the multigrid method against single grid calculations. For the cases here studied, they indicated that increasing the value of Re_{in} tends to increase the required computational effort. As far as the cycling strategy is concerned, results herein further suggested the existence of optimum numbers of coarsest-grid sweeps and of pre-/post-smoothing iterations. These numbers, however, cannot be easily determined a priori and may depend on specific characteristics of the flow in question.

Acknowledgement

The authors are thankful to CNPq, Brazil, for their financial support during the course of this research.

References

- [1] A. Brandt, Multi-level adaptive solutions to boundary-value problems, *Math. Comp.* 31 (138) (1977) 333–390.
- [2] W. Hackbusch, *Multigrid Methods and Applications*, Springer-Verlag, Berlin, 1985.
- [3] M. Hortmann, M. Peric, G. Scheuerer, Finite volume multigrid prediction of laminar convection: bench-mark solutions, *Int. J. Numer. Meth. Fluids* 11 (1990) 189–207.
- [4] B.R. Hutchinson, P.F. Galpin, G.D. Raithby, Application of additive correction multigrid to the coupled fluid flow equations, *Numer. Heat Transfer* 13 (1988) 133–147.
- [5] Y. Jiang, C.P. Chen, P.K. Tucker, Multigrid solutions of unsteady Navier–Stokes equations using a pressure method, *Numer. Heat Transfer—Part A* 20 (1991) 81–93.
- [6] S.V. Patankar, *Numerical Heat Transfer and Fluid Flow*, Mc-Graw Hill, 1980.
- [7] M. Peric, M. R ger, G. Scheuerer, A finite volume multigrid method for calculating turbulent flows, in: *Seventh Symposium on Turbulent Shear Flows*, Stanford University, 1989, pp. 7.3.1–7.3.6.
- [8] J.A. Rabi, M.J.S. de Lemos, Multigrid numerical solution of incompressible laminar recirculating flows, in: *ENCIT98- Proc. 7th Braz. Cong. Eng. Th. Sci.*, vol. 2, Rio de Janeiro, RJ, 3–6 November 1998, pp. 915–920.
- [9] J.A. Rabi, M.J.S. de Lemos, The effects of peclt number and cycling strategy on multigrid numerical solutions of convective–conductive problems, in: *7th AIAA/ASME Joint Thermo-physics and Heat Transfer Conf.*, Albuquerque, New Mexico, USA, 15–18 June 1998, Paper AIAA-98-2584.
- [10] J.A. Rabi, M.J.S. de Lemos, Optimization of convergence acceleration in multigrid numerical solutions of conductive–convective problems, *Appl. Math. Comput.* 124 (2001) 215–226.
- [11] J.A. Rabi, M.J.S. de Lemos, Multigrid correction-storage formulation applied to the numerical solution of incompressible laminar recirculating flows, *Appl. Math. Modelling* (in press).
- [12] P.S. Sathyamurthy, S.V. Patankar, Block-correction-based multigrid method for fluid flow problems, *Numer. Heat Transfer - Part B* 25 (1994) 375–394.
- [13] K. St ben, U. Trottenberg, Multigrid methods, in: *Lect. Notes Math.*, vol. 960, 1982, pp. 1–76.